Effect of Electrostatic Force Truncation on Interfacial and Transport Properties of Water

Scott E. Feller and Richard W. Pastor

Biophysics Laboratory, Center for Biologics Evaluation & Research, Food & Drug Administration, Rockville, Maryland 20852-1448

Atipat Rojnuckarin

Department of Chemical Engineering, University of Wisconsin—Madison, Madison Wisconsin 53706

Stephen Bogusz

Department of Gastroenterology, Walter Reed Army Institute of Research, Washington, DC 20307

Bernard R. Brooks*

Laboratory of Structural Biology, Division of Computer Research & Technology, National Institutes of Health, Bethesda, Maryland 20892

Received: May 21, 1996; In Final Form: August 2, 1996[⊗]

The importance of accurately accounting for all Coulombic forces in molecular dynamics simulations of water at interfaces is demonstrated by comparing the Ewald summation technique with various spherical truncation methods. The increased structure induced by truncation methods at 12 Å leads to water/vapor surface tensions and surface potentials that are respectively 50% and 100% greater than obtained with Ewald. The orientational polarization of water at the lipid/water interface is analyzed within the Marcelja−Radic theory of the hydration force, yielding decay parameters of 2.6 and 1.8 Å for spherical truncation and Ewald, respectively, as compared with 1.7−2.1 Å obtained from experiment. Bulk water transport properties such as the viscosity and diffusion constants differ by as much as 100% between simulations carried out with and without truncation; this may be related to ordering in the neighborhood of the cutoff radius. The diffusion constant calculated from the Ewald simulation is significantly further from experiment than the cutoff result, pointing out the need to reparametrize the TIP3P water model for use with Ewald summation. Appendices describe a method for carrying out the Ewald summation on a distributed memory parallel computer and other computational details relevant when simulating large systems.

I. Introduction

The calculation of the electrostatic energy of a periodic system, as is required in a molecular dynamics (MD) simulation using periodic boundary conditions, involves a double summation over the N charge sites (atoms) and their infinite number of periodic images. For point charges $\{q_n\}$ at position $\{r_n\}$ in an orthogonal unit cell of lengths L_x, L_y, and L_z, the potential energy is

$$U = \frac{1}{2}\sum_{i=1}^{N}\sum_{j=1}^{N} q_i q_j \sum_{l=0}^{\infty}\sum_{m=0}^{\infty}\sum_{n=0}^{\infty}{}' \frac{1}{|\vec{r}_{ij} + \vec{a}|} \qquad (1)$$

where

$$\vec{a} = (lL_x, mL_y, nL_z) \qquad (2)$$

is the lattice vector and the prime denotes the omission of self-energy terms, i.e., where $|\vec{r}_{ij} + \vec{a}| = 0$. (For molecular systems, pairs separated by one or two bonds are also excluded.)

As will be reviewed in the following section, eq 1 can be evaluated with good accuracy and efficiency using the Ewald (EW) summation technique. Nevertheless, because this is typically the most time-consuming part of an MD simulation, two other methods have been extensively employed to avoid the exhaustive summation of charge: (i) minimum image (MI) boundary conditions, where only pairs separated by a distance less than the simulation cell length are included; (ii) spherical boundary conditions (SBC), where either the potential or the force is truncated (abruptly or by employing a termination function) at a separation distance, r_c, typically 8−14 Å. Early simulation studies primarily concerned uncharged Lennard-Jones fluids, which were adequately treated using MI or SBC even when periodic boundary conditions (PBC) were employed. After artifacts due to truncation of charges were discovered in simulations of dipolar fluids, the Ewald method was largely adopted in the 1970s by liquid-state physicists. In contrast, issues involving Ewald summation were not even relevant for much of the biophysics community: because of the huge amount of solvent that must be included when modeling a biopolymer (e.g., protein or DNA) in PBC, until relatively recently, most simulations were carried out in vacuum, in a "droplet" of water, or with stochastic boundary conditions. As a result, the large biopolymer simulation programs evolved using SBC and continue to support the method even as reports of difficulties accumulate.[1−8] A review of the various boundary conditions and their effects on molecular simulations is found in ref 9.

The principal artifact associated with truncation of electrostatic forces in simulations is that of increased structure as compared with Ewald simulations. In simulations of polar fluids, increased orientational structure is observed,[10] dielectric properties are severely changed,[11] and both translational and rotational motion are decreased.[12] The effect is even more

[⊗] Abstract published in *Advance ACS Abstracts,* September 15, 1996.

S0022-3654(96)01465-7 CCC: $12.00

severe when simulating charged species; e.g., the radial distribution of electrolytes shows severe distortion in the vicinity of the cutoff.[9] The present study primarily concerns interfacial and transport properties, which will be shown to be especially sensitive to cutoff of the potential. In the next section we briefly describe the Ewald summation technique, and in three subsequent sections we compare results obtained with SBC and Ewald sums for bulk water, water at its vapor interface, and a hydrated lipid bilayer. Appendices discuss some technical details of MD simulations utilizing the Ewald summation, including an efficient parallelization scheme for use with distributed memory computers.

II. Ewald Summation Algorithm

The Ewald summation technique involves splitting the very slowly converging eq 1 into two more rapidly convergent sums. Briefly, two Gaussian charge distributions of opposite sign and arbitrary variance proportional to κ^{-2} are added at each point source of charge in the system. The first, which is opposite in sign to the original charge site, is denoted the screening distribution: when it is summed in real space along with the original charge distribution, the electrostatic interactions between charge sites become short ranged. The second, denoted the canceling distribution, maintains electroneutrality. It is summed in reciprocal space, and the total is then transformed back into real space. The net electrostatic potential energy is written

$$U = \frac{1}{2}\sum_{i=1}^{N}\sum_{j=1}^{N} q_i q_j \sum_{l=0}^{\infty}\sum_{m=0}^{\infty}\sum_{n=0}^{\infty}{}' \frac{\mathrm{erfc}(\kappa|\vec{r}_{ij}+\vec{a}|)}{|\vec{r}_{ij}+\vec{a}|} - \frac{\kappa}{2\sqrt{\pi}}\sum_{i=1}^{N}\sum_{j=1}^{N} q_i q_j \delta_{ij} + \frac{1}{2}\sum_{i=1}^{N}\sum_{j=1}^{N} \frac{q_i q_j}{\pi L_x L_y L_z} \sum_{l=0}^{\infty}\sum_{m=0}^{\infty}\sum_{n=0}^{\infty}{}' \frac{\exp\left(-\frac{|\vec{k}|^2}{4\kappa^2}\right)\cos(\vec{k}\cdot\vec{r}_{ij})}{|\vec{k}|^2} + J(D,\epsilon') \tag{3}$$

where $\vec{k}$ is the reciprocal space lattice vector

$$\vec{k} = 2\pi(l/L_x, m/L_y, n/L_z) \tag{4}$$

and erfc is the complementary error function. The first and third terms in eq 3 correspond to the real space and reciprocal space summations, respectively. Through the use of trigonometric identities, the double sum over atoms in the reciprocal space term can be converted to a single sum.[13] The real space summation includes atom pairs separated by a distance less than r_c. The reciprocal space sum is truncated at an ellipsoidal boundary (k_x^{max},k_y^{max},k_z^{max}). Both with κ determining the relative rates of convergence. (Increasing κ accelerates convergence of the real space sum but necessitates the inclusion of more terms in the reciprocal space sum.) The second term in eq 3 corrects for the self-energy of the canceling charge. The last term is a surface correction term that depends on the dipole moment of the unit cell, D, and the dielectric constant of the surrounding medium, ϵ'.[14] This term vanishes if one assumes that the entire system is surrounded by a conductor, i.e., $\epsilon' = \infty$. The effect of the surface term on simulations of aqueous electrolytes is discussed extensively in ref 15. For a more general discussion of the Ewald summation and references to its mathematical details, see ref 16.

In general, the computational expense in evaluating the electrostatic energy via eq 3 is of order N^2, though optimizing κ can lead to an efficiency of order $N^{3/2}$.[17] Recently developed algorithms utilizing interpolation[18,19] methods or fast Fourier transforms[20] to calculate the reciprocal space sum have an efficiency of order N ln N. The CHARMM (Chemistry at HARvard Molecular Mechanics)[21] implementation of the Ewald sums algorithm employed for the present work is based on the code given in refs 13 and 16 and is described further in Appendices A and B.

III. Simulation Details

All simulations were carried out with the CHARMM simulation package using the potential energy parameter set PARM22b4b.[22] A modified TIP3P water model[23] was used with the bonds and angle held rigidly with the SHAKE algorithm.[24] Three-dimensional periodic boundary conditions were employed for all systems. Simulations of bulk water and of water/vapor interfaces were carried out at constant particle number, volume, and energy (NVE) at a temperature of 293 K. Lipid bilayer simulations were carried out at constant normal pressure, surface area, and temperature (NPAT),[25] i.e., the length of the simulation cell in the direction normal to the interface (assumed to be z) varied to maintain a hydrostatic pressure of 1 atm. All simulations employed the leapfrog Verlet algorithm with a time step of 1 fs. Coordinate sets were saved every 100 fs for subsequent analysis.

The bulk water and water/vapor systems consisted of 560 water molecules. The periodic cell for the bulk water simulations was cubic with length 25.6 Å, corresponding to the experimental density of water at the simulation temperature. Ten separate 800 ps trajectories, five with Ewald and five with a 12 Å shifted potential, were generated; this relatively large amount of data was required to distinguish the two cutoff methods with high statistical certainty. In the water/vapor systems, the x and y dimensions were 25.6 Å, but the cell length normal to the interface (the z direction) was 75 Å. With this large region of vacuum above the water surface, the system is essentially periodic in only two dimensions though molecules which evaporate do pass through to the opposite side of the slab. Each water/vapor simulation was run for 300 ps. The lipid bilayer simulation cell contained 72 molecules of dipalmitoylphosphatidylcholine (DPPC) and 2511 water molecules. (Further details of the system and the SBC simulation can be found in ref 26.) The bilayer simulation using EW is a continuation of the SBC lipid simulation. The lipid simulations were carried out at a temperature of 323 K, corresponding to the liquid crystalline (L_α) state.

Simulations of water/vapor were performed using three spherical truncation methods: potential shifting (SH), where the electrostatic potential energy between each pair is scaled by $(1 - r^2/r_c^2)^2$; force switching (FSW), where the force is smoothly truncated to zero at the cutoff distance over a given range (2 Å in our simulations); and force shifting (FSH), where a constant is added to the force so that the potential is zero at the cutoff distance. Details of each of these methods are reviewed in ref 6. Cutoff distances of 12, 15, and 18 Å were tested for the truncation methods. The SBC simulations of bulk water and lipid bilayers were carried out with the 12 Å SH potential. Ewald sums were employed for simulations of each system using $r_c = 12$ Å, $\kappa = 0.210$ Å^{-1}, and $k^{max} = k_x^{max} = k_y^{max} = k_z^{max} = 4$. For the interfacial systems, which were in orthorhombic rather than cubic simulation cells, the number of wavevectors in the direction normal to the interface ($k_z^{max} = 11$ for water/vapor and 9 for water/lipid) was increased over those parallel ($k_x^{max} = k_y^{max} = 4$ for water/vapor and 6 for water/lipid) to obtain accurate energies and forces.[27] These parameters led

TABLE 1: Viscosity As Calculated from Eq 7 and the Diffusion Constant (Eq 5) for Each of the Bulk Water Simulations[a]

	viscosity (cP)		D (10^{-5} cm^2 s^{-1})	
simulation	12 Å SH	EW	12 Å SH	EW
1	0.70	0.37	4.01	5.03
2	0.52	0.41	3.96	5.10
3	0.54	0.30	3.77	5.18
4	0.68	0.33	3.75	5.15
5	0.66	0.38	3.93	4.99
av	0.62	0.35	3.88	5.09
std dev	0.08	0.04	0.17	0.08

[a] The experimental values are 1.0 cP and 3.0×10^{-5} cm^2 s^{-1}.

to relative force errors of order 10^{-4}. (The calculation is described in Appendix C.) The Lennard-Jones interactions were truncated at the cutoff distance with a smooth switching of the potential over a 2 Å region.

IV. Properties of Bulk Water

Liquid water is often used as a model system for testing the force truncation methods of biomolecular simulation. The choice is natural not only because many simulations are carried out in water but also because its properties tend to be very sensitive to any changes in the potential. This section describes results for the self-diffusion constant, viscosity, oxygen−oxygen radial distribution function, and dielectric constant of water.

The self-diffusion constant, D, was obtained from the final 400 ps of each simulation trajectory using the Einstein relation[16]

$$\langle |r_i(t) - r_i(0)|^2 \rangle = 6Dt \tag{5}$$

where $r_i(t)$ is the position of the ith water molecule at time t and the brackets denote the time average over the simulation length. At each value of t, the average and standard deviation of the displacement was determined from the 560 water molecules. The diffusion constant was then calculated from a fit in the region from 1.0 to 100.0 ps using the standard deviations as weights.[28] The use of a weighted fit makes the choice of the upper limit of the fitting interval largely irrelevant because the standard deviations of the long time points are very much larger than those at short time. The choice of the lower limit is somewhat arbitrary: it must be large enough to eliminate short time rattling motions but should also be kept as small as possible because the accuracy of the dependent variables deteriorates as time increases. The calculated diffusion constants are $(3.9 \pm 0.2) \times 10^{-5}$ cm^2 s^{-1} for SBC and $(5.1 \pm 0.1) \times 10^{-5}$ cm^2/s for EW; standard errors were estimated from the standard deviation among the five independent trajectories (Table 1). Both methods overestimate the experimental value of 3.0×10^{-5} cm^2 s^{-1}.

The viscosity was calculated from the integral of the pressure autocorrelation function via the Green−Kubo relation[29]

$$\eta = \lim_{t\to\infty} \frac{V}{k_B T} \int_0^t \langle P_{\alpha\beta}(0)\, P_{\alpha\beta}(t') \rangle \, dt' \tag{6}$$

where $P_{\alpha\beta}$ are the off-diagonal elements of the instantaneous pressure tensor (xy, xz, or yz). The pressure was saved every 2 fs during the simulation and the autocorrelation function evaluated (Figure 1a). The cumulative integral of the correlation function is shown in Figure 1b for integration times up to 1.0 ps. A difficulty in calculating viscosities from the Green−Kubo relation is the choice of upper integration limit because the long time tail of the correlation function contains a large degree of uncertainty.

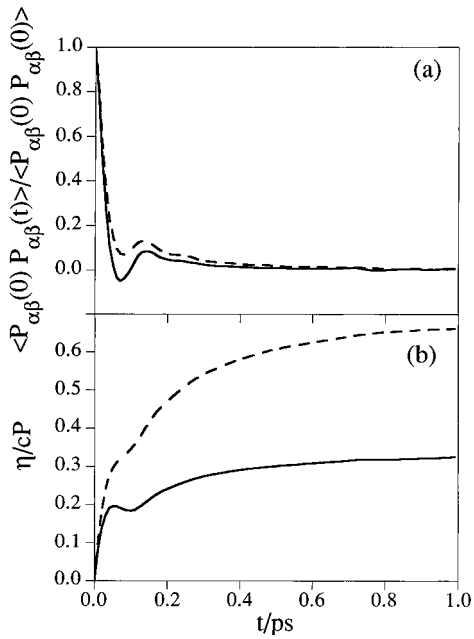

Figure 1. (a) Normalized pressure autocorrelation function for the Ewald (solid line) and SH (dashed line) truncation methods. (b) Viscosity as calculated from the cumulative integral of the pressure autocorrelation functions in (a).

Alternatively, the viscosity can be determined from the Einstein−Helfand relation[30,31]

$$\frac{2\eta kT}{V} t = \left\langle \left[\int_0^t P_{\alpha\beta}(t')\, dt' \right]^2 \right\rangle \tag{7}$$

To calculate the viscosities from the simulation, the right-hand side of eq 7 was calculated for each off-diagonal element and then averaged, the standard deviation among the three elements was determined, and the average in the interval $t = 1-100$ ps was fitted to eq 7 using the standard deviations as weights (as described in the calculation of the diffusion constant). Table 1 reports the average values and the standard deviations of the viscosity obtained from the 10 different simulations. The viscosities from the simulations employing spherical truncation (0.62 ± 0.04 cP) are approximately twice as large as those from the Ewald simulations (0.35 ± 0.02 cP) and are closer to experiment (1.0 cP). The viscosities as determined from the Green−Kubo relation (Figure 1b), though not as precise, are in qualitative agreement with the Einstein−Helfand results. The observation that the diffusion constant decreased while the viscosity increased is in accord with the Stokes−Einstein relation.

Figure 2 shows the oxygen−oxygen radial distribution function, $g(r)$, as evaluated from the simulations. Good agreement is found between the force treatments for the first few water shells ($r \approx 8$Å), but at greater distances the truncation method induces ordering into the fluid where the EW $g(r)$ is unity. As is clear from the inset of Figure 2, the differences between the distribution functions are statistically significant. The absence of the artifactual structuring in the EW simulations is consistent with the decrease in viscosity and the increase in diffusion constant over that observed in the SBC simulations.

The increased fluid structure in the region of the cutoff also leads to unphysical values of the dielectric constant when SBC are used.[11,15] The dielectric constant of the water model was

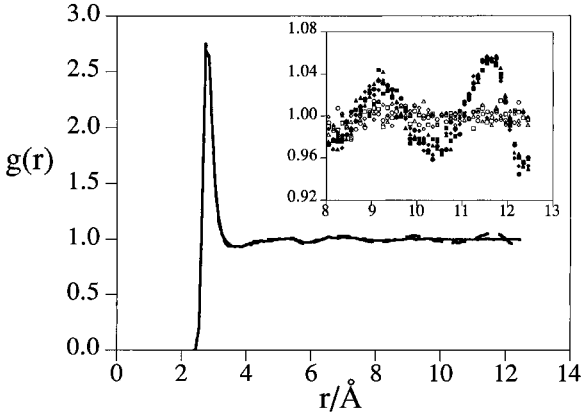

Figure 2. Oxygen−oxygen radial distribution function. The solid and dashed lines are the average of four EW and SH simulations, respectively. The inset shows the results of the individual simulations, the empty and filled symbols are the EW and SH results, respectively.

TABLE 2: Water/Vapor Surface Tension as a Function of Long-Range Force Treatment[a]

truncation method	γ (dyn/cm)	truncation method	γ (dyn/cm)
Ewald sum	52.7 ± 1.5	SH (12 Å)	70.2 ± 1.7
FSH (12 Å)	52.5 ± 1.3	SH (15 Å)	60.2 ± 1.7
FSW (10−12 Å)	43.8 ± 2.1	SH (18 Å)	54.6 ± 1.6

[a] The surface tension was calculated from eq 9, details on the calculation of the error bars are found in ref 25. The experimental value is 72.8 dyn/cm.

determined from the EW simulations using the relation[16]

$$\epsilon = 1 + \frac{4\pi}{3Vk_BT}\left(\left\langle\left|\sum_{i=1}^{N}\mu_i^2\right|\right\rangle - \left\langle\left|\sum_{i=1}^{N}\mu_i\right|\right\rangle^2\right) \qquad (8)$$

where μ_i is the dipole moment of water. A value of 109.5 was calculated compared to the experimental value of 80.4 at 293 K.[32]

V. Properties of the Water/Vapor Interface

The water/vapor interface has been studied by many workers using different water models and truncation schemes for the handling of Coulombic interactions[25,27,33] (see ref 33 for a review of the literature). We previously observed that the water/vapor interface was more sensitive to the choice of truncation radius than the liquid/liquid interface.[25] Thus, this system can serve as a sensitive test of the simulation results on force truncation method as we show for surface tension, configurational polarization, and surface potential.

For each truncation method, the interfacial tension was calculated during the simulation from the pressure tensor of the system,[25]

$$\gamma = {}^1/_2\langle L_z(P_{zz} - {}^1/_2(P_{xx} + P_{yy}))\rangle \qquad (9)$$

and is listed in Table 2. Fifty percent differences are observed between cutoff schemes even though the truncation lengths are longer than has typically been used for simulations on this system. Inclusion of all electrostatic interactions through the Ewald summation leads to a surface tension (52.7 dyn/cm) which is roughly 25% lower than the experimental values (72.8 dyn/cm). Using the SPC/E water model and Ewald sums, Alejandre et al. calculated a surface tension at 328 K which is in excellent agreement with experiment.[27] The density of the SPC/E water model at atmospheric pressure is also in better agreement with experiment than the TIP3P, possibly explaining the discrepancy between the experimental surface tension and that of the TIP3P model.

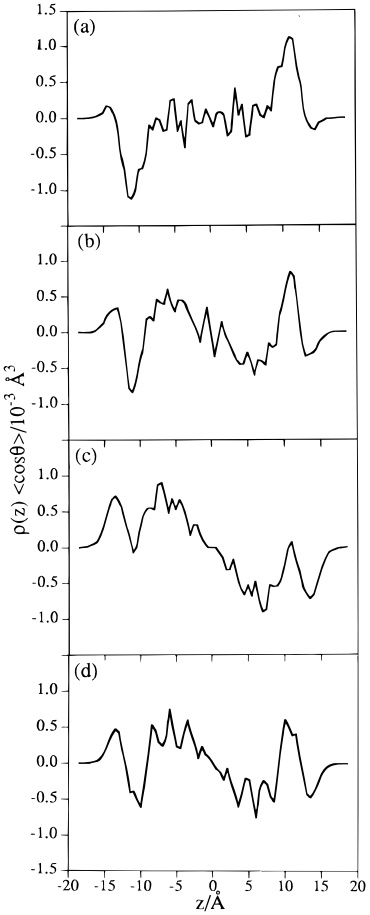

Figure 3. Density-weighted water polarization profiles for the water/vapor interface using different treatments of the electrostatic force: (a) EW, (b) 12 Å SH, (c) 12 Å FSH, and (d) 10−12 Å FSW

A particularly useful quantity that describes the atomic level structure of the water/vapor interface is the orientation of the water molecule dipole moment in the region of the interface. (In the bulk the distribution is uniform.) The product of the water density and the average z component of the dipole moment is plotted as a function of position along the z axis in Figure 3a for the EW simulation. The center of the water slab is located at $z = 0$, and the interfaces are approximately at $z = \pm 15$ Å. Analysis of the distribution of dipole vectors near the interface shows that the preferred orientation is parallel to the interface, similar to previous observations.[25,33] The distribution, however, is slightly skewed with the hydrogens pointed slightly into the vapor in the outermost layer and then more strongly oriented into the bulk water in the remainder of the interfacial region, leading to small net dipole moments. As shown in Figure 3, this distribution is extremely sensitive to the treatment of the long-range electrostatic force. In contrast to the EW simulation, where the perturbation extends to only two molecular diameters, the SBC simulations show ordering across the entire slab. The effect of increasing the cutoff radius with the shifted potential (which gave results closest to EW for this property) is illustrated in Figure 4, indicating that the artificial ordering due to truncation is reduced but clearly not eliminated even at 18 Å.

The nonuniform distribution of dipoles at the water/vapor interface leads to a mean electrostatic potential difference between liquid and vapor, often referred to as the surface potential.[34] The electrostatic potential along the interface normal

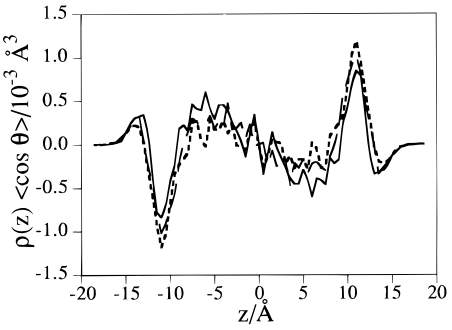

Figure 4. Density-weighted water polarization profiles for the water/vapor interface using the SH function with cutoff radius of 12 Å (solid), 15 Å (long dash), and 18 Å (short dash).

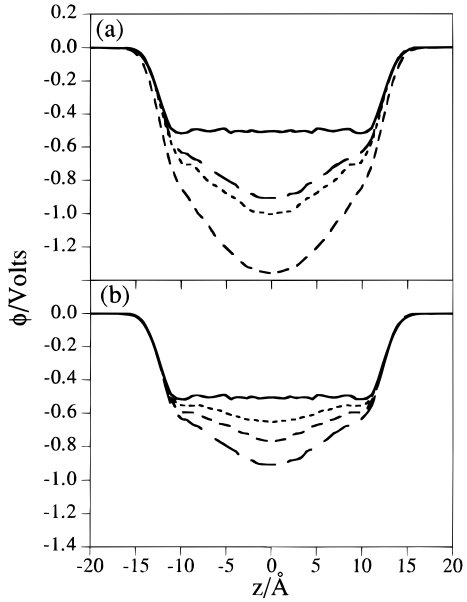

Figure 5. Electrostatic potential profile, as calculated from eq 10, for the water/vapor interface: (a) using EW (solid), 12 Å SH (long dash), 12 Å FSH (medium dash), and 10−12 Å FSW (short dash); (b) using the SH function with cutoff distances of 12 Å (long dash), 15 Å (medium dash), and 18 Å (short dash). The EW result is repeated in (b) for comparison purposes.

was calculated by double integration of Poisson's equation,

$$\phi(z) - \phi(0) = -\frac{4\pi}{\epsilon_0}\int_0^{\infty} dz' \int_0^{z'} dz'' \, \rho_c(z'') \qquad (10)$$

after binning the time-averaged charge density (ρ_c) as a function of z. To accomplish this, we divided the simulation cell into regions of 0.5 Å thickness and calculated the charge density in each slab averaged over the simulation length. The potential profile evaluated from the EW simulation is shown in Figure 5a (solid line). A potential drop of approximately 500 mV is seen upon moving from the vapor into the liquid; it occurs over the same 6 Å region where the density profile is changing. Figure 5a shows the electrostatic potential profile calculated with various truncation methods, and Figure 5b shows the effect of increasing cutoff radius with the potential shift method. The results are analogous to those for the dipole distribution, i.e., the potential drop occurs over a much longer range when the forces are truncated, leading to surface potentials which are up to 100% larger than the EW result. The region between 6 and 12 Å from the center reveals another difference between the EW and SBC simulations: the potential is nonmonotonic in the EW simulation. This indicates a reversal of the sign of the electric field, a result which is not reproduced by any of the SBC simulations. Additionally, the simulation using Ewald sums alone had a region of zero electric field and no ordered water at the center (Figure 3a); i.e. the two interfaces are interacting in the cutoff simulations. This is a serious consideration since one is typically trying to model two isolated interfaces with this geometry.

VI. Properties of the Water/Lipid Interface

After a brief review of the hydration force, results on polarization, potential drop, and surface tension of the bilayer/water interface are presented.

Hydration Force: Background. The study of phospholipid bilayers is a very active area of macromolecular simulation.[35] Primarily this is due to the importance of these systems as models for cell membranes, but they also have been studied both experimentally[36] and theoretically[37] by workers interested in the forces acting between hydrated surfaces. The existence of a hydration component in the force between solid surfaces was postulated following the observation of an anomalous exponential repulsion between mica sheets separated by only a few water diameters. These same types of measurements have been made for lipid bilayers at various temperatures and compositions.[36] A model for what is now commonly termed the hydration force was proposed by Marcelja and Radic, who assumed that water molecules are structured by the presence of the surface, with the ordering described by a parameter η. The free energy density of the system is given by a Landau expansion in η

$$f = f_0 + a\eta^2 + c(\partial\eta/\partial z)^2 \qquad (11)$$

where z is the direction normal to the interface and a and c are undetermined coefficients. With symmetric interfaces each a distance $h/2$ from the center, the minimization of the free energy (eq 11) leads to a differential equation

$$\frac{d^2\,\eta(z)}{dz^2} - \frac{a}{c}\eta(z) = 0 \qquad (12)$$

which subject to the relevant boundary conditions has solution

$$\eta(z) = \eta_0 \frac{\sinh(z/\lambda)}{\sinh(h/2\lambda)} \qquad (13)$$

where $\lambda = (c/a)^{1/2}$. With the free energy given by eq 11 and the order parameter described by eq 13, the repulsive hydration force between the surfaces is predicted to exponentially decay with decay length λ. Values of λ equal to 1.7 and 2.1 Å for L_α phase DPPC bilayers have been reported by McIntosh and Simon[38] and Rand and Parsegian,[36] respectively; the interpretation of force measurements and subsequent estimation of λ for lipid bilayers is complicated by the presence of undulations, which accounts for the slight discrepancy in these values.

Though the physical observable corresponding to the order parameter in the original Marcelja−Radic theory was not specified, later work related this parameter to the polarization of water.[39] Kjellander and Marcelja[40] and Berkowitz and Raghavan[41] subsequently investigated the orientational polarization of water in MD simulations of model lipid bilayers, calculating the order parameter as

$$\eta'(z) = \langle \cos\theta(z) \rangle \qquad (14)$$

where θ is the angle between the water dipole and the normal to the interface. An oscillatory decay was observed in both studies, implying that the water polarization was not the relevant

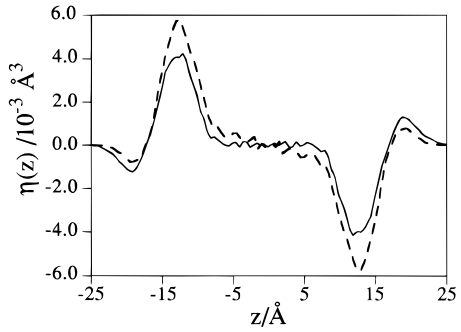

Figure 6. Density-weighted water polarization profiles for the water/lipid interface using the EW (solid) and 12 Å SH (dashed).

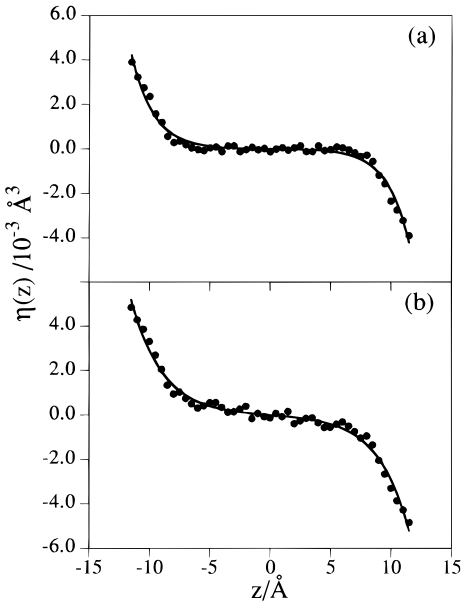

Figure 7. Fit of the density-weighted water polarization profiles to the form of the order parameter in the Marcelja−Radic hydration force theory: (a) EW, (b) 12 Å SH. The points are the simulation data, and the solid line is the best fit to the data.

order parameter. Following Wilson and Pohorille,[42] we have used an alternative function to represent the water ordering

$$\eta(z) = \langle \rho(z) \cos \theta(z) \rangle \tag{15}$$

This form gives a better description of the water interface by normalizing for the probability of a water molecule existing at a given location in *z*. This is the same form used in the previous section to describe polarization at the water/vapor interface.

Hydration Force: Results. Figure 6 plots $\eta(z)$ for the EW and SH simulations of the L_α DPPC bilayer. The center of the water lamella is located at $z = 0$, and the phosphatidylcholine headgroups are at approximately ± 16 Å. This plot shows that most of the perturbed water has its positively charged hydrogen atoms pointing toward the negatively charged phosphate groups. The perturbation of water acts over a much longer range when the spherical boundary conditions are used, in accord with our results for the free water surface. The SBC results, in contrast to the EW case, show little or no bulk water in the center of the cell although at this water concentration the lipids are known experimentally to be in excess water. The solid lines in Figure 7 represent the fit of the simulation results to the order parameter solution given by Marcelja and Radic (eq 13) over the region from -12 to 12 Å. This is the region where the slope and concavity of the data are the same as those of the fitting function and corresponds to the region where the density of water is 90% or more of its bulk value. The EW results yield a decay length of 1.8 Å, in excellent agreement with the aforementioned experimental measurements of the decay length of repulsive pressures between liquid crystalline bilayers, while the SBC simulation gives a significantly higher value of 2.6 Å.

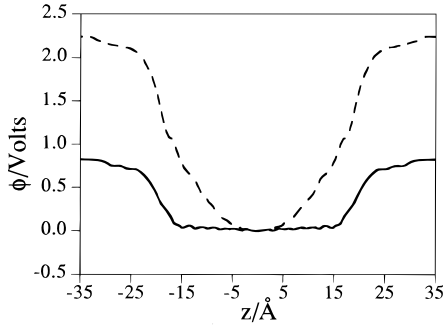

Figure 8. Electrostatic potential profile, as calculated from eq 10, for the water/lipid interface using EW (solid) and 12 Å SH (dashed).

TABLE 3: Water/Vapor, Water/Octane, and Water/Lipid Surface Tension from Simulations Using the 12 Å SH and EW Potentials[a]

system	12 Å SH	Ewald
water/vapor	70.2 ± 1.7	52.7 ± 1.4
water/octane	61.5 ± 1.5	46.6 ± 2.4
water/lipid	62.3 ± 2.8	42.9 ± 2.8

[a] The surface tension (in dyn/cm) was calculated from eq 9; details on the water/octane system and the calculation of the error bars are found in ref 25. The experimental values for the surface tension of water/vapor and water/octane are 72.8 and 51.7 dyn/cm, respectively.

Electrostatic Potential Drop. Figure 8 plots the electrostatic potential profile for the two bilayer simulations. Though the EW simulation yields a potential drop (800 mV) which is approximately twice the value expected from experiment, it is significantly better than the 2300 mV dipole potential obtained with spherical boundary conditions. The most striking difference between the two results is that the potential change occurs entirely in the phosphatidylcholine headgroup and carbonyl regions when the forces are not truncated, but extends out into the water layer when truncation is employed. Sensitivity of the dipole potential to cutoff artifacts has also been observed in previous lipid simulations. Zhou and Schulten[43] reported that the potential drop across a DLPE bilayer decreased by a factor of 7 when the fast multipole algorithm (FMA)[44] was used to calculate the coulombic forces instead of a spherical truncation at 8 Å. Berkowitz and co-workers reported that the dipole potential changed sign upon switching from SBC to Ewald sums.[45]

Bilayer Surface Tension. Bilayer surface tensions were calculated from the pressure anisotropies using eq 9. It is important to note that the "microscopic" surface tension of a small simulation cell may differ from that of a macroscopic membrane and is a function of the surface area.[46] The bilayer surface tension calculated with Ewald sums is 42.9 ± 2.8 dyn/cm, nearly 20 dyn/cm less than was calculated with SBC at the identical value of the surface area. The effect of force truncation on surface tension for water/vapor, water/octane, and water/lipid interfaces is summarized in Table 3.

VII. Discussion and Conclusions

We have examined the effects of force truncation on the structure and dynamics of bulk water and on the structure of water at planar interfaces. The observation common to all the systems is that long-range ordering of the fluid is increased when force truncation is employed. This possibly unintuitive result may be qualitatively understood by considering the nature of

the surroundings outside the cutoff radius. With SBC the system outside the cutoff sphere appears to be a vacuum, and thus it is as if each molecule is at the center of a tiny droplet. In behavior analagous to the water/vacuum systems studied in section V, the water within the cutoff sphere takes on an artificial ordering. In the bulk water simulations, the structuring was clearly demonstrated by the shape of the radial distribution function in the vicinity of the cutoff radius. This led to a greater viscosity and a lower translational diffusion constant for the SBC simulation compared to EW. The structure of water at its vapor interface, as described by the orientation of the water dipole vector with the surface normal, is artificially extended several molecular diameters into the water slab when the force is truncated. This leads to dipole potentials that are 50−100% greater than the EW result. Similar results are obtained for the structure of the water/lipid interface: the decay length of the water polarization was analyzed in terms of the Marcelja−Radic theory of the hydration force, and while the EW simulation results are in excellent agreement with the experimentally determined value, the SBC simulation yielded a value which was significantly higher. The surface tension of each type of interface also showed a strong dependence on the treatment of the Coulombic forces.

For the water/vapor simulations, no spherical truncation technique evaluated here reproduced the no cutoff simulation (EW). It should be noted that all the SBC methods tested here are atom-based; i.e., the inclusion of an atom pair for the interaction list is based solely on the distance between atoms. This is to be distinguished from the class of truncation methods (often referred to as group or residue based) where the interaction list includes all members of small groups whose group−group distance is less than the cutoff radius. Generally the groups are defined so as to be relatively small and electrically neutral. (Large force errors are observed if the groups have a net charge.[6]) For systems such as water, where each molecule can form a group, this approach is straightforward. For complex macromolecules, however, the designation of small neutral groups is arbitrary and sometimes requires adjustment of atomic partial charges to maintain efficiency.

In comparing the SBC methods for water/vapor, the worst results were obtained with the force shift method and the best with the potential shift (Figure 5a). Interestingly, Wodak and co-workers, in their simulations of *bulk* water, found good agreement between force shift and Ewald summation for both structural and dynamic quantities and found that the shifting function gave poor results.[47] Our simulations using the SH method showed that increasing the cutoff radius reduces the magnitude of the force errors but does not eliminate them even at $r_c = 18$ Å (Figure 5b). However, at this cutoff radius the SBC simulation is more expensive than the EW simulation with $r_c = 12$ Å.

In conclusion, force truncation leads to significant ordering that effects transport and surface properties. Altering the truncation termination function or the cutoff radius had little effect compared to the inclusion of all Coulombic interactions by way of the Ewald summation. The relatively poor results for surface tension, diffusion constant, and viscosity for pure water indicate that when Ewald summation is adopted, improvements in the TIP3P water model (originally parametrized using SBC at $r_c = 8$ Å) are required. In contrast, very good results with Ewald were obtained for the surface tension of the water/octane interface and the Marcelja−Radic parameter of the lipid bilayer. While these are important tests of the potential energy functions, further validation will ultimately be required when the water model is replaced.

Acknowledgment. We thank Pete Steinbach for critical discussions, Tom Darden for providing the PME code, and Milan Hodoscek for assistance with CHARMM parallelization. This research is supported in part by the Phillips Laboratory, Air Force Material Command, USAF, through the use of the IBM SP2 at the Maui High Performance Computing Center, and the Laboratory of Computational Biosciences, Division of Computer Research and Technology, NIH, through the use of the Intel Gamma. A.R. is supported by Office of Naval Research Grant N00014-92-J-1564 and National Science Foundation Grant CTS-9218668 and is grateful to Sangtae Kim for encouraging these efforts.

Appendix A. Parallelization of the Ewald Summation in CHARMM

To evaluate the real space sum in eq 3, an atom-based pair list which includes all neighbors out to a distance r_c plus a buffer region (typically 2 Å) is generated periodically during the simulation. The pair list is efficiently parallelized for distributed memory computing using the methods previously described for simulations with spherical boundary conditions.[48] The calculation of the complementary error function is discussed in Appendix B.

At each time step during the simulation, the reciprocal space summation (term 3 in eq 3) is calculated in two steps. First, a table is constructed of $\cos(\vec{k}\cdot\vec{r})$ for the x, y, and z positions of every atom at each value of l, m, and n, respectively. For p processors operating in parallel, each node is responsible for the calculation and storage of $1/p$th of the table with the partitioning done over atoms. In the second part of the calculation the electrostatic energy is estimated by summing over the reciprocal space vectors. For each wavevector, an inner loop over the N atoms is carried out using the cosine table calculated previously; i.e., the ordering of the inner and outer loops is the reverse of that in eq 3. The parallelization is done over atoms; i.e., each processor computes the inner loop only over the atoms for which it is responsible. The reciprocal space contribution to the electrostatic energy is determined by summing over processors at the end of the energy call (in the same way as is done for spherical cutoff simulations). The parallel version of the force calculation, however, is more complicated because the calculation of the force contribution for a given wavevector requires that the sum over all the atoms is available, and each processor only has the partial sum calculated from its subset of atoms. A global sum can be carried out for each wavevector before the force is calculated, but this increases the communication cost and is very inefficient for a large number of processors. An alternative is to calculate the partial sum over atoms for each wavevector, store these values, and then do a single global sum after going through all the wavevectors. At this point the force can then be calculated by again summing over each wavevector and atom. This second approach reduces communication overhead but requires the recalculation of some $\cos(\vec{k}\cdot\vec{r})$ terms. The second approach is thus preferable for computers with a large number of processors and/or large communication latency times. The first approach, because it requires fewer floating point operations, is more efficient for the smaller number of nodes typical of workstation clusters. For the simulations of a hydrated lipid bilayer, described in section VI, the crossover point was found to be eight nodes on an IBM SP2.

Though the parallelization schemes for the reciprocal space summation are not nearly as elegant as the real space sum, we find that for large systems remarkable efficiency is obtained, e.g., 1 ps simulations of the hydrated lipid bilayer simulations

(17 000 atoms) took 2.7 h on four processors and 10.8 h on a single processor. These simulations were carried out on a cluster of HP9000/735 series workstations connected by an FDDI ring. One hundred percent efficiency is observed in the parallelization because of reduced time to access the arrays which hold the cosine tables (which are much smaller since each node only stores the elements for its atoms). Greater than 100% efficiency was observed in simulations of a 10 500-atom hydrated gel-phase lipid bilayer (see ref 49 for details of the simulation). These efficiencies are especially impressive since spherical truncation simulations of the same systems yield only a 75% parallelization efficiency.

Appendix B. Methods To Calculate erfc

Six methods (denoted as methods I to VI) were tested for computing the erfc function. Methods I and II use a continued fraction development of the incomplete gamma function as outlined in section 6.2 of ref 28. In these methods two separate summations are used, one of which converges faster at small values of r and a second which is more rapid at large r. Method I uses double precision representation in the calculations and iteratively computes erfc until changes in the value are on the order of the double precision representation. Method II employs the same algorithm as method I but uses a single precision iteration criteria.

Methods III and IV employ polynomial expansions. Method III uses a polynomial expansion multiplied by an exponential;[51] method IV uses a Chebyshev polynomial expansion inside the exponential (section 6.2 of ref 28).

Methods V and VI use a look-up table of erfc values generated at the beginning of the simulation using method I. Method V uses linear interpolation to estimate the erfc value while method VI uses cubic spline interpolation. These methods require a memory allocation of approximately 200 kB, much less than 1% of the capacity of modern workstations.

To test these methods, the forces were calculated for one dynamics frame from a 200 ps simulation of a periodic 55 Å cubic system consisting of a hydrated protein fragment from the crystal structure of the human class II histocompatability molecule[51] (180 amino acids, 4585 water molecules, and 8 counterions for a total of almost 17 000 atoms). Each of the erfc methods was used to calculate the forces on each atom. The accuracy of each method was estimated by comparing these forces with those obtained from the high-precision iterative technique (method I). This high-accuracy calculation was performed with $r_c = 20$ Å, $\kappa = 0.250$, and $k^{max} = 20$. This calculation is too computationally expensive for routine use in MD simulations but can be used as a standard in estimating errors. The error in the forces were used (instead of the error in the energies) because the forces are used to calculate positions in molecular dynamics; such errors would thus propagate through the length of the simulation.

The average errors in the forces for these methods are shown in Table 4. In column 2 the parameters of the calculation were the same as the high-accuracy calculation described above; only the erfc method was varied. In the third column, the calculation was repeated with a set of parameters that more reasonably balance computational time and accuracy: $r_c = 16$ Å, $\kappa = 0.180$, and $k^{max} = 7$. The relative force error reported is the root-mean-squared difference between the calculated forces and the high-accuracy results, divided by the average force on each atom. From column 2 we see that the single precision calculation (method II) and the cubic spline interpolation (VI) give the smallest deviations from the method I results, with the linear interpolation method (V) having the largest error by far.

TABLE 4: Relative Force Errors (rms) for Both High and Medium Accuracy Calculations for Each of the erfc Calculation Methods Tested Here[a]

method	high accuracy	medium accuracy (computational time in h)
I (high precision)		1.26×10^{-4} (6.14)
II (low precision)	1.94×10^{-8}	1.26×10^{-4} (4.08)
III (ref 51)	1.01×10^{-6}	1.26×10^{-4} (2.94)
IV (Chebyshev)	4.48×10^{-7}	1.26×10^{-4} (3.29)
V (linear interpolation)	2.97×10^{-4}	1.96×10^{-4} (2.75)
VI (cubic spline)	2.58×10^{-8}	1.26×10^{-4} (2.80)

[a] The average relative force error is the root-mean-squared difference between these force calculations divided by the average force on each atom. Times shown are for 100 steps of dynamics at medium accuracy.

TABLE 5: Relative Force Errors (rms) for Various Values of the Maximum Number of Reciprocal Lattice Vector[a]

k^{max}	rel force error (rms)	k^{max}	rel force error (rms)
2	4.70×10^{-2}	8	2.46×10^{-3}
3	3.66×10^{-2}	9	1.15×10^{-3}
4	2.56×10^{-2}	10	5.21×10^{-4}
5	1.62×10^{-2}	11	2.05×10^{-4}
6	9.39×10^{-3}	12	7.97×10^{-5}
7	5.04×10^{-3}	13	3.19×10^{-5}

[a] For each calculation $\kappa = 0.180$ and $r_c = 16$ Å.

TABLE 6: Relative Force Errors (rms) for Various Values of κ, with $k^{max} = 7$ and $r_c = 16$ Å

κ	rel force error (rms)	κ	rel force error (rms)
0.1	2.13×10^{-2}	0.24	1.53×10^{-3}
0.12	7.91×10^{-3}	0.26	2.94×10^{-3}
0.14	2.36×10^{-3}	0.28	5.04×10^{-3}
0.16	5.64×10^{-4}	0.3	7.92×10^{-3}
0.18	1.26×10^{-4}	0.32	1.17×10^{-2}
0.2	2.44×10^{-4}	0.34	1.63×10^{-2}
0.22	6.81×10^{-4}		

In medium accuracy calculations (second column of Table 4) the differences in relative error between II, III, IV, and VI are nearly identical and thus are not the deciding factor in choice of method. The computational time required for 100 steps of molecular dynamics is shown in the last column of Table 4. The linear interpolation method requires the least time, but is the least accurate and is not recommended. The cubic spline interpolation method requires only slightly more time and is significantly more accurate. These results are machine dependent, although timing results using a 16-node parallel computation on an IBM SP2 machine gave similar trends, with the cubic spline also found as the method of choice (data not shown).

Appendix C. Choice of Parameters and Errors in Ewald Calculations

Increasing either r_c or k^{max} increases both accuracy and computational time in Ewald calculations. The accuracy as a function of k^{max} can be seen in Table 5. Choice of κ for a given cutoff distance also affects accuracy, but in a more complex way than either r_c or k^{max}. As κ is increased, the force errors decrease, reaching a minimum at $\kappa = 0.180$ and then increasing again (Table 6). As κ does not affect the computational time of the simulation, one should choose the value giving the greatest accuracy for a given r_c and k^{max}.

To determine which set of parameters would be the most efficient for a given size system, one must first decide what level of error in the forces are acceptable. An arbitrary level of 2×10^{-4} was chosen for this appendix. For each value of k^{max} between 6 and 13, the minimum value of r_c and the corresponding κ value which gave force errors of 2×10^{-4} or

TABLE 7: Computational Time Required for 100 Steps of Molecular Dynamics for Each Value of k^{max} between 6 and 13 Using the Shortest Spherical Cutoff Distance (and Corresponding κ Value) Such That Average Relative Force Errors of Less Than 2×10^{-4} Were Achieved

k^{max}	r_c	κ	rel force error (rms)	time/100 steps dynamics (h)
6	18	0.16	1.17×10^{-4}	3.12
7	16	0.18	1.26×10^{-4}	2.94
8	15	0.20	8.57×10^{-5}	3.23
9	14	0.22	7.76×10^{-5}	3.72
10	14	0.24	7.37×10^{-5}	4.61
11	13	0.24	5.74×10^{-5}	5.49
12	11	0.28	1.30×10^{-4}	6.48
13	10	0.30	1.86×10^{-4}	11.12

TABLE 8: Computational Time Required for 100 Steps of Molecular Dynamics for Values of Grid Density between 0.35 and 1.77 (Corresponding to Division of the System into 20 to 100 Grids in Each Direction)[a]

grid density/ Å^{-1}	order of interpolation	r_c	κ	rel force error (rms)	time/100 steps dynamics (h)
0.35	10	16	0.20	3.81×10^{-5}	2.33
0.53	8	14	0.24	1.64×10^{-5}	1.49
0.71	8	10	0.32	4.72×10^{-5}	0.95
0.88	6	10	0.32	4.41×10^{-5}	0.77
1.06	6	10	0.34	2.91×10^{-5}	0.82
1.27	6	10	0.36	2.65×10^{-5}	0.83
1.77	4	10	0.34	4.31×10^{-5}	0.92

[a] For each grid density, r_c, κ, and the interpolation order were optimized to yield the shortest computational time for average relative force errors of less than 2×10^{-4}.

TABLE 9: A Comparison of the Relative Force Errors (rms) of Three Spherical Cutoff Methods, Shift, Force Shift, and Force Switch, at Different Cutoff Distances[a]

r_c	shift	force switch	force shift	
10	8.33×10^{-2}	7.38×10^{-2}	3.89×10^{-2}	(0.45)
12	5.97×10^{-2}	5.95×10^{-2}	2.87×10^{-2}	(0.62)
14	4.51×10^{-2}	5.14×10^{-2}	2.25×10^{-2}	(0.87)
16	3.51×10^{-2}	4.40×10^{-2}	1.82×10^{-2}	(1.20)
18	2.80×10^{-2}	3.89×10^{-2}	1.51×10^{-2}	(1.58)

[a] The computational time shown is in parentheses for 100 steps of MD using the force shift method.

less were determined. Molecular dynamics runs of 100 steps were then performed on the system using these Ewald parameter sets and the computational time compared (Table 7). The most effective set of parameters was found to be $\kappa = 0.180$, $k^{max} = 7$, and $r_c = 16$ Å, which required 2.9 h for 100 dynamics steps on a Hewlett-Packard 735 workstation. The timing results in Table 7 vary by almost a factor of 4; thus, careful choice of the parameters can significantly decrease computational time. This result is system size dependent and also machine dependent; a similar optimization would be required in each individual case.

A recent refinement of the Ewald technique, the smooth particle mesh Ewald (PME) method,[19] decreases the time required to carry out the reciprocal space sum by employing interpolation techniques and fast Fourier transforms (FFT). The CHARMM implementation of the PME method is based on the code described in ref 19. For relative force errors of 2×10^{-4} with the system described here the computational time for 100 dynamics steps is decreased by a factor of 4 (Table 8). The PME method requires about the same computational time as a 13 Å SBC calculation (Table 9) with the accuracy increased by a factor of 1000.

The system used for the tests in Appendices B and C is contained in a cubic box of length 55 Å. When the simulation cell has sides of equal length, the values of k^{max} in each direction are the same. For anisotropic unit cells, such as the water/vapor interface (see section V), these values are optimized independently.

Finally, a comparison of the forces of the Ewald method with those of three spherical cutoff methods—shift, force shift, and force switch—is given in Table 9. Steinbach and Brooks[6] have shown that the FSH and FSW are more accurate than SH for treating the electrostatics of a hydrated protein, and these findings agree with Table 9. Nevertheless, small but systematic errors can lead to important effects in a simulation (see section V where SH gave results which were closer to EW than either FSW or FSH). Table 9 demonstrates that even large spherical cutoff values cannot reproduce the accuracy of the Ewald calculations, making it the method of choice for periodic systems. The medium accuracy Ewald calculations reduced the force error by a factor of 100 or more over all the SBC methods.

References and Notes

(1) Shelley, J. C.; Patey, G. N. *Mol. Phys.* **1996**, *88*, 385.
(2) Klein, M. L.; McDonald, I. R. *J. Chem. Phys.* **1979**, *71*, 298.
(3) Alper, H. E.; Bassolino, D.; Stouch, T. R. *J. Chem. Phys.* **1993**, *98*, 9798.
(4) Tasaki, K.; McDonald, S.; Brady, J. W. *J. Comput. Chem.* **1993**, *14*, 278.
(5) Roberts, J. E.; Schnitker, J. *J. Phys. Chem.* **1995**, *99*, 1322.
(6) Steinbach, P. J.; Brooks, B. R. *J. Comput. Chem.* **1994**, *15*, 667.
(7) Brooks, C. L.; Pettitt, B. M.; Karplus, M. *J. Chem. Phys.* 1**985**, *83*, 5897.
(8) Schreiber, H.; Steinhauser, O. *Biochemistry* **1992**, *31*, 5856.
(9) Smith, P. E.; van Gunsteren, W. F. Methods for the Evaluation of Long Range Electrostatic Forces in Computer Simulations of Molecular Systems. In van Gunsteren, W. F., Weiner, P. K., Wilkinson, A. J., Eds. *Computer Simulation of Biomolecular Systems: Theoretical and Experimental Applications*; ESCOM: Leiden, 1993; Vol. 2, pp 182−212.
(10) Pangali, C.; Rao, M.; Berne, B. J. *Mol. Phys.* **1980**, *40*, 661.
(11) Neumann, M. *Mol. Phys.* **1983**, *50*, 841.
(12) van Gunsteren, W. F.; Berendsen, H. J. C.; Rullman, J. A. C. *Faraday Discuss.* **1978**, *66*, 58.
(13) Smith, W. *CCP5 Inf. Q.* **1986**, 37.
(14) DeLeeuw, S. W.; Perram, J. W.; Smith, E. R. *Proc. R. Soc. London* **1980**, *A373*, 27.
(15) Roberts, J. E.; Schnitker, J. *J. Chem. Phys.* **1994**, 101, 5024.
(16) Allen, M. P.; Tildesley, D. J. *Computer Simulation of Liquids*; Clarendon: Oxford, 1987.
(17) Perram, J. W.; Petersen, H. G.; DeLeeuw, S. W. *Mol. Phys.* **1988**, *65*, 875.
(18) Darden, T.; York, D.; Pedersen, L. *J. Chem. Phys.* **1993**, *98*, 10089.
(19) Essmann, U.; Perera, L.; Berkowitz, M. L.; Darden, T.; Lee, H.; Pedersen, L. G. *J. Chem. Phys.* **1995**, *103*, 8577.
(20) York, D.; Yang, W. *J. Chem. Phys.* **1994**, *101*, 3298.
(21) Brooks, B. R.; Bruccoleri, R. E.; Olafson, B. D.; States, D. J.; Swaminathan, S.; Karplus, M. *J. Comput. Chem.* **1983**, *4*, 187.
(22) Schlenkrich, M.; Brickmann, J.; MacKerell, A. D.; Karplus, M. In *Biological Membranes*: *A Molecular Perspective from Computation and Experiment*; Merz, K. M., Roux, B., Eds.; Birkhauser: Boston, 1996; p 31.
(23) Durell, S. R.; Brooks, B. R.; Ben-Naim, A. *J. Phys. Chem.* **1994**, *98*, 2198.
(24) Ryckaert, W. E.; Ciccotti, G.; Berendsen, H. J. C. *J. Comput. Phys.* **1977**, *23*, 327.
(25) Zhang, Y.; Feller. S. E.; Brooks, B. R.; Pastor. R. W. *J. Chem. Phys.* **1995**, *103*, 10252.
(26) Feller, S. E.; Zhang, Y.; Pastor, R. W. *J. Chem. Phys.* **1995**, *103*, 10267.
(27) Alejandre, J.; Tildesley, D. J.; Chapela, G. A. *J. Chem. Phys.* **1995**, *102*, 4574.
(28) Press, W. H.; Teukolsky, S. A.; Vettering, W. T.; Flannery, B. P. *Numerical Recipies*; Cambridge University Press: New York, 1992.
(29) Green, M. S. *J. Chem. Phys.* **1954**, *22*, 398.
(30) Helfand, E. *Phys. Rev.* **1960**, *119*, 1.
(31) Smith, P. E.; van Gunsteren, W. F. *Chem. Phys. Lett.* **1993**, *215*, 315.
(32) Weast, R. C.; Astle, M. J.; Beyer, W. H. *CRC Handbook of Chemistry and Physics*; CRC Press: Boca Raton, FL, 1986.
(33) Pohorille, A.; Wilson, M. A. *J. Mol. Struct.* **1993**, *284*, 271.
(34) Goodisman, J. *Electrochemistry: Theoretical Foundations*; Wiley: New York, 1987.
(35) Pastor, R. W. *Curr. Opin. Struct. Biol.* **1994**, *4*, 486.
(36) Rand, R. P.; Parsegian, V. A. *Biochim. Biophys. Acta* **1989**, *988*, 351.

(37) Marcelja, S.; Radic, N. *Chem. Phys. Lett.* **1976**, *42*, 129.
(38) McIntosh, T. J.; Simon, S. A. *Annu. Rev. Biophys. Biomol. Struct.* **1994**, *23*, 27.
(39) Gruen, D. W. R.; Marcelja, S. *J. Chem. Soc., Faraday Trans. 2* **1983**, *79*, 225.
(40) Kjellander, R.; Marcelja, S. *Chem. Scr.* **1985**, *25*, 73. Kjellander, R.; Marcelja, S. *Chem. Phys. Lett.* **1985**, *120*, 393.
(41) Berkowitz, M. L.; Ragahavan, K. *Langmuir* **1991**, *7*, 1042.
(42) Wilson, M. A.; Pohorille, A. *J. Am. Chem. Soc.* **1994**, *116*, 1490.
(43) Zhou, F.; Schulten, K. *J. Phys. Chem.* **1995**, *99*, 2194.
(44) Board, J. A., Jr.; Causey, J. W.; Leathrum, J. F., Jr.; Windemuth, A.; Schulten, K. *Chem. Phys. Lett.* **1992**, *198*, 89.
(45) Essmann, U.; Perera, L.; Berkowitz, M. L. *Langmuir* **1995**, *11*, 4519.
(46) Feller, S. E.; Pastor, R. W. *Biophys. J.* **1996**, *71*, 1350.
(47) Prevost, M.; Van Belle, D.; Lippens, G.; Wodak, S. *Mol. Phys.* **1990**, *71*, 587.
(48) Hwang, Y; Das, R.; Saltz, J.; Hodoscek, Brooks, B. R. *IEEE Comput. Sci. Eng.* **1995**, *2*, 18.
(49) Venable, R. M.; Brooks, B. R.; Pastor, R. W., To be submitted.
(50) Abramowitz, M.; Stegun, I. A. *Handbook of Mathmatical Functions*; Dover Publications: New York, 1964.
(51) Stern, L. J.; Brown, H. J.; Jardetzky, T. S.; Gorga, J. C.; Urban, R. G.; Strominger, J. L.; Wiley, D. C. *Nature* **1994**, *368*, 215.

JP9614658